LAWRENCE
LIVERMORE
NATIONAL
LABORATORY

LLNL-JRNL-413920

Studies of Shear Band Velocity Using Spatially and Temporally Resolved Measurements of Strain During Quasistatic Compression of Bulk Metallic Glass

W. J. Wright, M.W. Samale, T.C. Hufnagel, M.M. LeBlanc, J.N. Florando

June 15, 2009

Acta Materialia

Disclaimer

Studies of Shear Band Velocity Using Spatially and Temporally Resolved Measurements of Strain During Quasistatic Compression of a Bulk Metallic Glass

Wendelin J. Wright[1], M.W. Samale[1], T.C. Hufnagel[2], M.M. LeBlanc[3], and J.N. Florando[3]

[1]Santa Clara University, Dept. of Mechanical Engineering, Santa Clara, CA 95053

[2]Johns Hopkins University, Dept. of Materials Science and Engineering, Baltimore, MD 21218

[3]Lawrence Livermore National Laboratory, Livermore, CA 94550

Keywords: Metallic glasses; shear band velocity; plastic deformation; compression test.

Abstract

We have made measurements of the temporal and spatial features of the evolution of strain during the serrated flow of $Pd_{40}Ni_{40}P_{20}$ bulk metallic glass tested under quasistatic, room temperature, uniaxial compression. Strain and load data were acquired at rates of up to 400 kHz using strain gages affixed to all four sides of the specimen and a piezoelectric load cell located near the specimen. Calculation of the displacement rate requires an assumption about the nature of the shear displacement. If one assumes that the entire shear plane displaces simultaneously, the displacement rate is approximately 0.002 m/s. If instead one assumes that the displacement occurs as a localized propagating front, the velocity of the front is approximately 2.8 m/s. In either case, the velocity is orders of magnitude less than the shear wave speed (~2000 m/s). The significance of these measurements for estimates of heating in shear bands is discussed.

Introduction

During quasistatic compression testing performed at a constant displacement rate at temperatures well below the glass transition, the plastic strain in bulk metallic glasses is accommodated by thin shear bands [1–10]. As a shear band propagates, the displacement rate of the material in the band exceeds the displacement rate imposed on the sample. Consequently, the load drops, and the load train and the sample elastically recover. Numerous repetitions of these

events cause the characteristic "serrated flow," commonly observed during uniaxial compression of bulk metallic glasses [11–17].

The nature of shear banding is a focus of research in the metallic glass community. Areas of interest include the structure of shear bands [7, 10, 18–23], strategies for enhancing the plastic strain accommodated by shear bands [24–30], the amount of heating that occurs in shear bands during deformation [16, 17, 31–33], and the velocity of the propagating shear bands [4, 5, 16, 17, 33, 34].

These last two topics – heating in shear bands and shear band velocity – are inextricably linked and have critical implications for the underlying deformation mechanism. One of the earliest attempts at measuring shear band velocity in bulk metallic glasses was made by Neuhäuser who used high–speed cinematography to record the development of shear bands during deformation of metallic glass ribbons [4]. Some shear bands initiated and propagated from one frame to the next, therefore placing an upper bound limit on the shear band propagation time as the time elapsed between frames or 1.7 ms – 2.5 ms for two different alloys. Using a model for which shear happens simultaneously along the entire length of the shear band, the shear band velocity was estimated as 40 μm/s. The resolution of these measurements was later improved by Hampel and Neuhäuser through the use of an optoelectronic technique in which an optical microscope and photo cell captured images of the formation of shear steps on the surface of a metallic glass ribbon deformed in bending [5]. The output of the photo cell was recorded by a digital oscilloscope, and the intensity was calibrated as a function of step height. The shear offsets at the surface of the sample measured normal to the sample surface ranged from 30 – 120 nm in length. The photo cell measurements indicated that these steps formed during a period of 15 – 100 μs. Hampel and Neuhäuser did not infer shear band velocities based on these measurements, presumably because in their experiment, the geometry of shear band propagation was complicated by the nature of the specimen, a thin metallic glass ribbon loaded in bending.

The shear band velocity is a key parameter in estimates of the local heating that occurs during shear band propagation; as expected, as shear band velocity increases, the predicted maximum temperature increases because less time is available for heat dissipation away from the shear band. Numerous reports have suggested that the temperature rise that occurs during shear band propagation may be sufficient to reach the glass transition temperature or even the melting temperature of bulk metallic glasses [34–38]. The notion that significant local heating may occur during shear band propagation in bulk metallic glasses was first proposed by Leamy, Chen, and Wang who attributed the vein pattern morphology of fracture surfaces to adiabatic heating of the deformed region [35]. Later Liu and co–workers detected sparking from tension samples during the moment of fracture and observed liquid droplets at major cracks adjacent to the fracture surfaces [36]. By assuming that all of the elastic strain energy stored in a sample at the moment of tensile fracture was dissipated as heat on the fracture plane, they estimated temperature increases of 900 K. This hypothesis gained further support based on the results of dynamic compression testing by Bruck, Rosakis, and Johnson [37]. Temperature increases of nearly 775 K were observed using high–speed infrared detection. It should be noted, however, that the calculated or measured temperature increases cited here are applicable to fracture events and do not necessarily apply to the inhomogeneous deformation that occurs prior to failure. Also infrared temperature measurements do not have the spatial and temporal resolution necessary to directly measure the maximum temperature increases. Instead, calculations must be performed to infer the maximum temperature increase experienced by the shear band. For example, Jiang and co–workers performed infrared temperature measurements during plastic deformation of $Zr_{52.5}Cu_{17.9}Ni_{14.6}Al_{10.0}Ti_{5.0}$ [38]. The temperature measurements had a spatial resolution of 10 μm and were captured at a frequency of 1000 Hz. The maximum temperature increases measured using infrared thermography were at most 3 K for a strain rate of 2.8×10^{-2} m/s. The authors used Fourier's law of heat conduction to match theoretical profiles to the experimentally

determined temperature profile perpendicular to a shear band (across its thickness) with the heat content of the shear band as the fitting parameter. They then calculated the maximum temperature increase in the shear band using the heat content estimation and assuming that shear bands propagate with a velocity equal to ninety–percent of the transverse speed of sound in the solid. In so doing, they calculated temperature increases of several thousand degrees Kelvin. We reiterate, however, that such high temperatures have never been directly measured.

More recently Lewandowski and Greer performed a series of experiments in which a tin coating was deposited on double–notched four–point bend bulk metallic glass specimens [31, 32]. The sample was loaded until fracture with failure occurring near one of the notches. Melting of the tin deposit was observed at the notch that did not fail, indicating that the shear bands that formed there experienced temperature increases of more than 200 K. Lewandowski and Greer used their coupled temperature and mechanical measurements to make extrapolations of the peak temperature rises that occur in shear bands [31, 32]. In so doing, they report temperature increases in excess of 1000 K using a thin film solution for a heat source that operates instantaneously; however, we note that as the elapsed time during shear band propagation increases, the predicted temperature rise decreases. It should also be noted that shear bands were observed that did not cause melting of the tin [32], and it is unclear as to whether the shear bands at which the tin melted formed prior to sample failure during serrated flow or during the final failure event.

In this work, we describe the culmination of a series of experiments that have been performed over a number of years [16, 17, 33]. One of the goals of these experiments has been to determine the shear band velocity during quasistatic uniaxial compression. The earliest measurements lacked the temporal and spatial resolution necessary to conclusively determine the shear displacement rate [16, 17]. Displacement was measured as the sample average using linear variable differential transformers, and the data were acquired at a rate of 100 Hz. Only a lower

bound for shear band velocity could reasonably be determined from this data. Later Wright performed a series of experiments in which strain gages were applied to two opposing sample faces during quasistatic compression [33]. The spatial resolution was improved in that the strain gages had an active grid length of only 800 μm. The strain gage amplifier included 1.6 kHz active low pass filters, meaning that the instrumentation could accurately track events that occurred with an elapsed time as short as 625 μs, and the data were acquired at a rate of 5 kHz. This work indicated that the time elapsed during the propagation of a single shear band across a sample with a width of 2 mm at an angle of approximately 45˚ to the loading axis was on the order of 1 ms. These data provided some evidence that shear bands were not deforming as rapidly as the shear wave speed in the solid as has been often assumed in the literature [31, 38], but the frequency response of the strain gage amplifier was comparable to the characteristic time for the events being studied. The experiments were also complicated by sample bending during compression. (Note that recently Chen and co–workers and Song and Nieh performed similar experiments in which they applied strain gages to a variety of bulk metallic glass specimens tested under quasistatic uniaxial compression, and the serrated flow was measured at a data acquisition rate of 2 kHz. This work also indicates an elapsed time of ~1 ms during the displacement increment of a single serration for Pd based and Mg based [39] and Zr based bulk metallic glasses [40].)

Thus the work described herein was undertaken. Quasistatic compression testing was performed on samples of amorphous $Pd_{40}Ni_{40}P_{20}$ with strain gages applied to all four faces parallel to the loading axis and using a specially designed high–stiffness testing fixture. The data were acquired at rates up to 400 kHz, and the lowest cutoff frequency for the instrumentation was –3 dB at 100 kHz. Great care was taken to avoid sample bending through control of sample tolerances and design of the loading apparatus (and, in fact, the use of strain gages on opposing sides of the specimen demonstrates that the bending is minimal as we show below). Based on

this data, the shear displacement rates during shear banding events are measured, and a range of shear band velocities is estimated. The precise value of the shear band velocity depends on assumptions about the manner in which the shear is accomplished.

Experimental Procedures

An ingot of $Pd_{40}Ni_{40}P_{20}$ was prepared by induction melting Pd and Ni_2P in an argon atmosphere and suction casting [41]. The ingot was amorphous as confirmed by a single broad x–ray diffraction peak acquired using a Philips APD3720 diffractometer. Samples with a length of 6 mm in the direction of the loading axis and an aspect ratio of 3:1 were electrode discharge machined from the cast material using low power and water cooling to prevent crystallization. Tight tolerances were imposed on the sample dimensions to minimize bending of the samples during compression. The square 2 mm x 2 mm faces to which the compressive load was to be applied were ground parallel to within 1 μm. The faces oriented parallel to the loading axis were machined perpendicular to the loading faces to within 5 μm. The faces oriented parallel to the loading axis were mechanically polished to a 0.05 μm surface finish in order to facilitate observation of shear bands and to remove damage due to the machining process.

Quasistatic uniaxial compression tests were performed on amorphous $Pd_{40}Ni_{40}P_{20}$ samples using a screw–driven Instron 1127 mechanical test system. A diagram of the load train is shown in Figure 1. The tests were performed with a nominal strain rate of 10^{-4} s^{-1}. The load data were acquired using a 250 kN Instron load cell and a Kistler piezoelectric load cell with a 180 kHz bandpass filter. The piezoelectric load cell was placed approximately 25 mm below the sample. A piezoelectric load cell was chosen because it could be placed in close proximity to the sample and because it experiences less mechanical ringing than a conventional load cell due its high stiffness and higher frequency response. The sample was loaded by cylindrical 10 mm diameter tungsten carbide platens that were constrained to coaxial alignment by a steel sleeve with two concentric holes. A steel ball placed in the load train in a truncated conical cavity at the

top of the upper tungsten carbide platen facilitated parallel alignment of the platens. The displacement was acquired using an MTS extensometer attached to the loading platens.

Prior to mechanical testing, it was determined that the load train stiffness was not sufficiently high to permit sustained plastic flow of the specimens [42, 43]. We have observed that if a load train does not have a stiffness of at least 10^8 N/m, $Pd_{40}Ni_{40}P_{20}$ bulk metallic glass samples with the dimensions used in this work will simply fail during the propagation of one of the first serrations. This is related to a transfer of elastic energy from the load train, which is not infinitely stiff, to the sample during the load drop, thereby driving the shear band to the point of failure [43]. Thus the load train had to be modified to increase its stiffness. To accomplish this, three aluminum pillars were inserted into the load train. The pillars were seated on the steel sleeve and surrounded the steel ball as shown in Figure 1. The height of the pillars was initially larger than the diameter of the steel ball. In order for the load to be transmitted through the steel ball and the tungsten carbide loading platens to the sample, the aluminum pillars first had to be compressed such that their height was reduced to that of the diameter of the steel ball. Load frames often exhibit bilinear stiffnesses with the stiffness of the load frame at low loads being lower than the stiffness of the load frame at high loads as shown in Figure 2. Thus by inserting the aluminum pillars into the load train, the total load imposed on the load train was increased significantly, thereby shifting the load frame stiffness to the higher stiffness regime. The stiffness of the modified load train was determined to be 1.5×10^8 N/m by measuring the load and displacement with no sample present. (Note that the load frame stiffness in the high stiffness regime obtained from Figure 2 is higher than 1.5×10^8 N/m because the measurements in Figure 2 were made without the elements of the load train shown in Figure 1 present.) With these modifications, the 250 kN Instron load cell measured the total load applied to the load train; the piezoelectric load cell located directly beneath the sample sensed only the load applied to the sample.

The key feature of the data acquisition was strain gages applied directly to all four of the sample faces that were oriented parallel to the loading axis. The strain gages were model 031DE from Vishay Micro–Measurements. They had a square active grid area (0.8 mm × 0.8 mm) that was centered along the length and width of each sample face. The wire material was Constantan, and the strain gages could measure a maximum strain of 3% for their gage length. The gages were self–temperature compensated, and a 350 Ω resistance was chosen to decrease leadwire effects and improve the signal–to–noise ratio in the gage circuit. Each strain gage was used in a quarter bridge configuration. The excitation voltage was 2.5 V. The strain gages were conditioned with Dynamics Universal Amplifiers (Model 7600A) with a frequency response of –3 dB at 100 kHz. The strain gages were labeled A1, B1, A2, and B2 such that the pair of gages A1 and A2 and the pair of gages B1 and B2 were affixed to opposite sides of the sample.

The data were simultaneously acquired using a Nicolet Vision recorder at data acquisition rates of 50 Hz and 100 kHz and sporadically with a Nicolet Integra 40 oscilloscope at 400 kHz. The identical data acquisition system has been used at the Lawrence Livermore National Laboratory for high strain rate Hopkinson bar testing. For Hopkinson bar testing of stainless steel, the strain gage recording the strain in the incident bar measured the time rate of change of the incident wave as 333 s^{-1}. It will be shown that this response rate is sufficient to accurately capture the temporal features of the shear band propagation. The same epoxy used to affix the strain gages to the bulk metallic glass samples was used to affix the strain gages for the Hopkinson bar testing, and, therefore, any viscoelastic behavior of the epoxy is not expected to affect the strain gage data. Two tests with fully gaged specimens were performed. For clarity, the results presented below will highlight one of these tests, but the results obtained from both tests are consistent with each other.

After testing, the locations of the active grid lengths of the strain gages were marked on the samples, and then the strain gages were removed. Fractured specimens were imaged using a Hitachi S–4800 field emission scanning electron microscope.

We reiterate the uniqueness of these measurements for testing of bulk metallic glasses: strain gages were placed directly on the sample surfaces to measure the temporal and spatial features of the strain with time, a piezoelectric load cell was located 25 mm from the sample, and the data were acquired at 400 kHz during serrated flow. In our experience, this degree of care in the experimentation is essential for accurate measurement of the temporal evolution of strain and load during rapid displacement events. Measurements with more conventional instrumentation are inadequate for this task.

Experimental Results

Figure 3 is a plot of true stress versus true strain for uniaxial compression of $Pd_{40}Ni_{40}P_{20}$. The load data are from the piezoelectric load cell, and the strain data are from the extensometer. The yield strength is 1.7 GPa, and the elastic modulus is 110 GPa. Figure 4 is a plot of engineering stress versus engineering strain showing the data from all four strain gages. Bending of the sample was minimal as the strain recorded by the four gages differed by less than 2% of the measured values.

Figure 5 is a plot of strain versus time for all four strain gages and the extensometer for a portion of the serrated flow. The sample sustained 0.1% plastic strain with eighteen measurable serrations over this time interval. The data shown in Figure 5 were acquired at a rate of 50 Hz. It is important to note that not all of the serrations that are observed using strain gages are visible in the extensometer data, which average over the entire sample length and have poorer resolution. Figure 6 comprises plots of strain versus time for all four strain gages. Each plot represents a single serration acquired at a rate of 100 kHz. The load data from the piezoelectric load cell are also shown. A corresponding load drop accompanies each serration observed in the strain data.

Figures 6(a) and 6(b) are representative serrations indicating that the elapsed time during the serration is on the order of 1 ms. The strain increments are as large as 350×10^{-6}. The strain rate during each serration is approximately 0.3 s^{-1} and thus is sufficiently low to be accurately captured by the strain gages. The four strain gages and the load cell indicate that the events appear to initiate simultaneously on the four strain gages to within an uncertainty of about 200 μs. We note that this uncertainty is significantly smaller than the interval over which the strain events evolve (~1 ms) but significantly larger than the time required for a shear wave to transit the specimen (~1 μs).

The strain gages record both tensile and compressive events. In Figure 6, an increment in strain, such as that shown for Gage A1 in Figure 6(a), represents an increase in the overall compressive strain or a compressive strain event. A decrement in strain, such as that shown for Gage A2 in Figure 6(a), represents a relaxation, or tensile event. Most serrations (fifteen of eighteen for this test) show one set of opposing strain gages recording events of opposite sign with tensile events or negligibly small strain events on the other set of gages as shown in Figure 6(a). Some serrations show all gages recording tensile events as shown in Figure 6(b), but no serrations show compressive events on two opposing gages. Note that the sign of the events changes on a single strain gage. For example, in Figure 6(a), Gage A1 records a compressive event whereas in Figure 6(b), the same strain gage records a tensile event. If these differences in sign were simply due to macroscopic sample bending, the signs of the events on a single strain gage would not be expected to change between serrations.

Figure 7 is a plot of strain versus time for all four strain gages for a single serration acquired at a rate of 400 kHz with an overlay of the corresponding 100 kHz data. The agreement between the two data sets is excellent. This is not surprising given that the signal conditioning filter on the strain gage amplifier is the same for both data sets, but the frequency of the data acquisition at 400 kHz is more than twice that of the frequency at which the strain gage amplifier

begins to attenuate the strain gage signals, thereby satisfying the Nyquist–Shannon sampling theorem [44, 45] and supporting the validity of the temporal measurements. (According to the Nyquist theorem, a signal must be sampled at least twice as fast as the frequency of the signal to accurately reconstruct the waveform. For example, a signal with a frequency of 1 kHz must be sampled at a frequency of at least 2 kHz; otherwise, the high–frequency content of the 1 kHz signal will appear (or alias) at a false lower frequency inside the spectrum of interest.)

Figure 8 comprises scanning electron micrographs of the sides of the sample to which Gages A1 and B1 were affixed. The circular marks indicate the corners of the active grid region of the strain gages. Notice that there is one primary shear band that is observable in these low magnification views, and it does not intersect the active grid regions. Even at higher magnifications, no shear bands were observed in the active grid regions. The fracture surface also does not intersect the active grid region as can be seen in Figure 8(b). Figure 9 is a magnification of the corner of side A1. The location of this image is marked in Figure 8(a). As seen in Figure 9, there are more shear bands visible than serrations recorded. These shear bands are likely due to local stress concentrations at the sample corners.

Discussion

Shear Band Velocity

The time elapsed during the unloading segment of a single serration is on the order of 1 ms in $Pd_{40}Ni_{40}P_{20}$. This measurement can be used to estimate the shear band velocity (*i.e.,* the relative displacement rate of material on either side of the shear band) although assumptions regarding the nature of shear band propagation must first be made. Figure 10 illustrates two models for shear band propagation. For a simultaneous shear model in which the shear band operates simultaneously across the entire shear plane producing a 2 μm shear offset at the sample surface, a velocity of $2\ \mu m / 1\ ms = 0.002$ m/s is calculated. Two microns is a typical value for shear offsets for compression samples of this size [16, 17, 38, 46]. For a progressive shear

model, in which the shear displacement occurs in a localized front that propagates across the specimen, the relevant length is the length of the shear band. For a sample with a width of 2 mm and shear bands that propagate at approximately 45˚ to the loading axis, the shear band velocity is estimated as $2\sqrt{2}$ mm / 1 ms $= 2.8$ m/s. It is clear that regardless of the nature of the shear, these velocities are many orders of magnitude smaller than the shear wave speed in bulk metallic glasses. For $Pd_{40}Ni_{40}P_{20}$, which has a shear modulus of 36.6 GPa and a density of $9.36\ g/cm^3$ [47], the shear wave speed is 1977 m/s. This range of shear band velocity (0.002 m/s – 2.8 m/s) is in agreement with the results from other groups that provide lower bound estimates for the shear band velocity [4, 5, 34, 39, 40].

Shear Band Heating

By assuming that all of the plastic work of a single serration is dissipated as heat during the propagation of a single shear band and using the measurements made here, the heat content in a single shear band is estimated as 2400 kJ/mol, in agreement with the measurements of other groups [31, 38, 48]. In making this calculation, a shear band thickness of 10 nm is assumed [19]. Models for shear band heating based on detailed measurements of serrated flow have been presented elsewhere based on both simultaneous and progressive shear models [16, 17]. The maximum temperature increase experienced by the shear bands is of primary interest. The progressive shear model predicts larger temperature increases than the simultaneous shear model because the plastic work causes a larger temperature increase when dissipated progressively over a small volume rather than simultaneously over the entire shear band. Thus the progressive shear model will be briefly reviewed here.

In the model for heating due to progressive shear, the boundary between the sheared and unsheared material is treated as a process zone in which heat is generated. It is assumed that the formation of each shear band manifests as a single serration and that all of the work done in producing the shear band is dissipated as heat. The heat source is modeled as a planar slit with

width $2a$ as illustrated in Figure 10(b). Heat is generated at the rate $\dot{Q}$ per unit time per unit length over the slit. $\dot{Q}$ is given by $\dot{Q} = \tau_{yield}\, u_{plastic}\, V$, where τ_{yield} is the applied shear stress, $u_{plastic}$ is the plastic displacement in the plane of the shear band, and V is the velocity of the heat source as it propagates across the sample. The velocity of the heat source is given by $V = l / \Delta t$, where l is the length of the shear band and Δt is the time elapsed during the unloading segment of a single serration. It is assumed that each shear band crosses the entire sample and is oriented at an angle φ with respect to the loading axis such that $l = w / \sin\varphi$ where w is the sample width in the direction of shear band propagation. (The angle φ is equal to 42˚ for $Pd_{40}Ni_{40}P_{20}$ [13, 14].) The half–width of the slit, a, is a measure of the width of the process zone. The half–width a is estimated according to the equation for the radius of the core of a screw dislocation, $a = u_{plastic} / (2\pi\gamma)$, where $u_{plastic}$ is the typical shear offset produced by a shear band and γ is the elastic strain that is supported by the glass at the yield stress. The elastic strain γ is given by $\gamma = \tau_{yield} / \mu$, where τ_{yield} is the shear yield strength of the material and μ is the shear modulus. It is critical to note that this model does not assume that the propagation of a shear band is analogous to the propagation of a dislocation in a crystalline material. The estimate for the size of the process zone a is based on an estimation of the shear distortion that will cause the glass to yield. The yield strength of the glass is exceeded for a smaller process zone size. Thus the size of the process zone is given by

$$a = \frac{u_{plastic}\mu}{2\pi\tau_{yield}}. \tag{1}$$

Using the parameters defined previously, the temperature change at a point for a planar heat source moving in the direction of the negative x–axis, as derived by Carslaw and Jaeger [49], is given by

$$\Delta T(x,z) = \frac{\dot{Q}}{4\pi K}\frac{1}{a}\int_{-a}^{a} \exp\left[\frac{V(x-x')}{2\kappa}\right] \mathrm{K}_0\left[\frac{V\sqrt{(x-x')^2+z^2}}{2\kappa}\right] dx', \tag{2}$$

where z is the position coordinate along the direction perpendicular to the plane of the shear band, K is the thermal conductivity, κ is the thermal diffusivity, and K_0 is the modified Bessel function of the second kind of order zero. The prediction of this model for the temperature profile in the plane of a shear band ($z = 0$), based on the data for a single serration and the thermal constants for $Pd_{40}Ni_{40}P_{20}$ [50], is shown in Figure 11. The values used to produce this plot are reported in Table 1. The heat source is moving in the negative x–direction, and there is a negligible temperature change in front of the heat source because that material has not yet sheared. The temperature profile is sharply peaked within the process zone region. There is a residual temperature increase behind the heat source because the material there has just sheared and the heat has not yet fully dissipated. The maximum temperature increase of 65 K is insufficient to reach the glass transition temperature of $Pd_{40}Ni_{40}P_{20}$ of 576 K [47], the critical temperature at which a dramatic decrease in viscosity due to heating would occur. The finite thickness of shear bands has not been incorporated into this model; if it were, the predicted temperature increase would be even smaller. This progressive shear analysis also assumes that all of the work done in forming the shear band is dissipated as heat. Some of this energy, however, is stored as strain energy [51], thereby decreasing the amount of heat produced and thus decreasing the peak temperature.

Some research suggests that a single serration may be representative of the collective propagation of multiple shear bands [38, 46, 52]. If this is the case, perhaps ten, or as an upper bound – even one hundred shear bands produce a single serration. If each of the shear bands propagates in succession across the entire width of the sample (an unlikely scenario), then perhaps the shear band velocity is in fact as much as 100 times faster than the displacement rates estimated here, but the shear band velocity would still be nearly an order of magnitude slower than the shear wave speed in the solid. To the authors' knowledge, there is no experimental confirmation of shear band velocity based on mechanical measurements to suggest that the shear

band velocity is faster than the velocities estimated here. Also, while microcompression experiments performed on the same alloy indicate that perhaps a few shear bands form per serration [52], there is no evidence to the authors' knowledge that dozens of shear bands form per serration. This low ratio of shear bands per serration is also consistent with bulk compression testing on other alloys [38]. If it is the case that multiple shear bands propagate sequentially during a single serration, then the shear band velocity may be higher than these measurements indicate; however, the plastic work done must then be partitioned amongst the shear bands. Figure 12 is a plot of the expected temperature profile assuming that ten shear bands produce a single serration. Each shear band propagates at a velocity ten times faster than the velocity assumed in Figure 11. The maximum temperature increase experienced by the shear band is 209 K in this case, which is insufficient to reach the glass transition temperature.

Although the temperature increases predicted for heating during serrated flow are small, SEM micrographs of the fracture surface of $Pd_{40}Ni_{40}P_{20}$ [16] suggest that significant localized heating occurs during the final, failure event. Since the magnitude of the load drop during failure is much larger than the magnitude of the load drops that occur during serrated flow, a larger temperature increase is expected. Furthermore, the data from the piezoelectric load cell for the second sample tested in these experiments indicate that the sample failure occurred over a period of 40 microseconds. Using the model for simultaneous shear [16], the temperature increase predicted for the final failure event in a $Pd_{40}Ni_{40}P_{20}$ sample exceeds the melting temperature of 991 K [47]. (Note that this increase is much higher than our earlier estimates [16, 17, 33] since the time resolution of the data acquisition has been significantly improved in this work.) Shear bands that form during the final failure event are expected to reach temperatures sufficiently high to melt a fusible tin coating on the sample surface and the glass itself.

The data shown here shed doubt on the use of the shear wave speed in estimates of local heating in shear bands and should raise questions as to whether temperatures during shear band

propagation *prior to specimen fracture* reach the glass transition temperature. Furthermore, recent work by other groups supports a simultaneous shear model [32, 53, 54]; for a simultaneous shear model, the expected temperature increases are lower than predicted here [16].

Sign of the Strain Events

The patterns observed in the sign of the strain events registered by the strain gages are striking. Typically events of opposite sign are registered on one pair of opposing strain gages with tensile events on the other pair. No compressive–compressive events are observed on opposing strain gages. The recurrence of tensile events on at least one pair of opposing strain gages for each serration suggests that the gages of the tensile pair are affixed to the sample faces that are oriented parallel to the direction of shear band propagation for each shear band. Recently a $Zr_{64.13}Cu_{15.75}Ni_{10.12}Al_{10}$ bulk metallic glass was observed to exhibit multiple serrations during a uniaxial compression test for which all of the serrations were attributed to deformation in a single shear band as evidenced by striations on the deformed surface as it protruded from the sample [54]. Such striations were not observed in this work. Furthermore, given that the signs of the strain events change on the strain gages during the test, it seems unlikely that all eighteen serrations can be attributed to the same shear band.

As the load drops during a serration, the metallic glass not contained in shear bands elastically recovers, i.e. the strain is tensile. If shear bands must intersect a strain gage in order to register a compressive event, then due to the geometry of the specimens used in this work, the location of the 0.8 mm gage length at the midpoint of the sample length, and the fact that shear bands formed during uniaxial compression in metallic glasses propagate at ~45˚ to the loading axis, compressive–compressive events cannot occur on a pair of opposing strain gages for a single serration. This is consistent with all available data. No shear bands were observed to intersect the active strain gage regions during scanning electron microscopy of the deformed specimens. This result suggests that shear bands have an associated strain field that is registered

by the strain gages as the shear band initiates and propagates; if this is indeed the case, it is not required that a shear band intersect a gage in order to be registered. Presumably fewer serrations than shear bands are observed because either the resolution of the instrumentation is such that not all shear banding events are recorded, or, as mentioned previously, the activity of multiple shear bands manifests as a single serration. Further work is underway in order to definitively explain the signs of the strain events that are observed. Understanding the strain field may provide an explanation as to why the operation of a single shear band does not necessarily cause catastrophic failure and the propagation of multiple shear bands can be sustained.

The strain gage data do not conclusively point to either a simultaneous or progressive shear model at this juncture. While the strain events as recorded by all four strain gages appear to begin and end at the same point in time and be concurrent with the load drops within the resolution of the instrumentation, this alone cannot confirm a simultaneous shear model. As a shear band initiates and propagates, the surrounding material experiences a simultaneous elastic unloading that would be registered by the strain gages as the consequence of the initiation of a progressive shear. High–speed image acquisition that documents shear band propagation across a sample may be necessary to confirm the nature of shearing in bulk metallic glasses.

Conclusions

The elapsed time during shear band propagation in amorphous $Pd_{40}Ni_{40}P_{20}$ was determined using strain gages. If shear happens along the entire length of the shear band simultaneously, the relative displacement rate of material on either side of the shear band is approximately 0.002 m/s. If instead the shear displacement occurs in a localized front that propagates across the specimen, the shear band velocity is approximately 2.8 m/s. For both cases, the shear band velocity is many orders of magnitude slower than the shear wave speed in the bulk metallic glass. Thermal modeling based on this range of shear band velocities predicts

maximum temperature increases of only 65 K in a shear band during serrated flow and temperature increases sufficient to melt the glass during the failure event.

Acknowledgements

The authors gratefully acknowledge the contributions of W.D. Nix to the early experiments that resulted in this work [16, 17]. The authors also thank S. Hruszkewycz for preparing the $Pd_{40}Ni_{40}P_{20}$ ingots. W.J. Wright and M.W. Samale were funded by the Lawrence Livermore National Laboratory under Subcontract B565228. T.C. Hufnagel gratefully acknowledges support from the National Science Foundation under grant DMR–0705517. The work of J.N. Florando and M.M LeBlanc was performed under the auspices of the U.S. Department of Energy by Lawrence Livermore National Laboratory under Contract DE–AC52–07NA27344.

References

[1] Pampillo CA, Chen HS. Mater Sci Eng 1974;13:181.

[2] Pampillo CA. J Mater Sci 1975;10:1194.

[3] Spaepen F. Acta Metall 1977;25:407.

[4] Neuhäuser H. Scripta Metall 1978;12:471.

[5] Hampel A, Neuhäuser H. Recording of Slip Line Development with High Resolution. In: Chiem CY, Kunze H–D, Meyer LW, editors. Impact Loading and Dynamic Behaviour of Materials, vol. 2. Oberursel (Germany): DGM Informationsgesellschaft, 1988. p. 845.

[6] Argon AS. Acta Metall 1979;27:47.

[7] Donovan PE, Stobbs WM. Acta Metall 1981;29:1419.

[8] Steif PS, Spaepen F, Hutchinson JW. Acta Metall 1982;30:447.

[9] Hufnagel TC, El–Deiry P, Vinci RP. Scripta Mater 2000;43:1071.

[10] Li J, Spaepen F, Hufnagel TC. Philos Mag A 2002;82:2623.

[11] Chen HS. Scripta Metall 1973;7:931.

[12] Kimura H, Masumoto T. Acta Metall 1983;31:231.

[13] Donovan PE. Mater Sci Eng 1988;98:487.

[14] Donovan PE. Acta Metall 1989;37:445.

[15] Bruck HA, Christman T, Rosakis AJ, Johnson WL. Scripta Metall Mater 1994;30:429.

[16] Wright WJ, Schwarz RB, Nix WD. Mater Sci Eng A 2001;319:229.

[17] Wright WJ, Saha R, Nix WD. Mater Trans JIM 2001;42:642.

[18] Flores KM, Suh D, Dauskardt RH, Asoka–Kumar P, Sterne PA, and Howell RH. J Mater Res 2002;17:1153.

[19] Li J, Wang ZL, Hufnagel TC. Phys Rev B 2002;65:144201.

[20] Kim J–J, Choi Y, Suresh S, Argon AS. Science 2002;295:654.

[21] Jiang WH, Atzmon M. Acta Mater 2003;51:4095.

[22] Jiang WH, Pinkerton FE, Atzmon M. J Appl Phys 2003;93:9287.

[23] Jiang WH, Atzmon M. Scripta Mater 2006;54:333.

[24] Donovan PE, Stobbs WM. J Non–Crystall Solids 1983;55:61.

[25] Hays CC, Kim CP, Johnson WL. Phys Rev Lett 2000;84:2901.

[26] Xing L–Q, Li Y, Ramesh KT, Li J, Hufnagel TC. Phys Rev B 2001;64:180201.

[27] Schroers J, Johnson WL. Phys Rev Lett 2004;93:255506.

[28] Donohue A, Spaepen F, Hoagland RG, Misra A. Appl Phys Lett 2007;91:241905.

[29] Kim KB, Das J, Lee MH, Yi S, Fleury E, Zhang ZF, Wang WH, Eckert J. J Mater Res 2008;23:6.

[30] Wang K, Fujita T, Zeng YQ, Nishiyama N, Inoue A, Chen MW. Acta Mater 2008;56:2834.

[31] Lewandowski JJ, Greer AL. Nature Mater 2006;5:15.

[32] Zhang Y, Stelmashenko NA, Barber ZH, Wang WH, Lewandowski JJ, Greer AL. J Mater Res 2007;22:419.

[33] Wright WJ. “Shear Band Processes in Bulk Metallic Glasses,” Doctoral Dissertation, Stanford University, 2003.

[34] Jiang WH, Fan GJ, Liu FX, Wang GY, Choo H, and Liaw PK. J Mater Res 2006;21:2164.

[35] Leamy HJ, Chen HS, Wang TT. Metall Trans 1972;3:699.

[36] Liu CT, Heatherly L, Easton DS, Carmichael CA, Schneibel JH, Chen CH, Wright JL, Yoo MH, Horton JA, Inoue A. Metall Mater Trans A 1998;29:1811.

[37] Bruck HA, Rosakis AJ, Johnson WL. J Mater Res 1996;11:503.

[38] Jiang WH, Liao HH, Liu FX, Choo H, Liaw PK. Metall Mater Trans A 2008;39:1822.

[39] Chen HM, Huang JC, Song SX, Nieh TG, and Jang JSC. App Phys Lett 2009;94;141914.

[40] Song SX, Nieh TG. Intermetallics 2009;doi:10.1016/j.intermet.2009.03.005.

[41] Kui HW, Greer AL, Turnbull D. App Phys Lett 1984;45:615.

[42] Murata T, Masumoto T, Sakai M. Rapidly Quenched Metals III 1978;2:401.

[43] Han Z, Wu WF, Li Y, Wei YJ, and Gao HJ, Acta Mater 2009;57:1367.

[44] Nyquist H. Proc IEEE 2002;90:280. Reprinted from Trans AIEE 1928;Feb:617.

[45] Shannon C. Proc IEEE 1998;86:447. Reprinted from Proc IRE 1949;37:10.

[46] Jiang WH, Liu FX, Liaw PK, Choo H. App Phys Lett 2007;90:181903.

[47] He Y, Shen T, Schwarz RB. Metall Mater Trans A 1998;29:1795.

[48] Bengus VZ, Tabachnikova ED, Shumilin SE, Golovin YI, Makarov MV, Shibkov AA, Miskuf J, Csach K, Ocelik V. Int J Rapid Solid 1993;8:21.

[49] Carslaw HS, Jaeger JC. Conduction of Heat in Solids. London: Oxford University Press, 1959, p.269.

[50] Harms U, Shen TD, Schwarz, RB. Scripta Mater 2002;47:411.

[51] Chen HS. Appl Phys Lett 1976;29:328.

[52] Schuster BE, Wei Q, Hufnagel TC, and Ramesh KT. Acta Mater 2008;56:5091.

[53] Packard CE, Schuh CA. Acta Mater 2007;55:5348.

[54] Song SX, Bei H, Wadsworth J, Nieh TG. Intermetallics 2008;16:813.

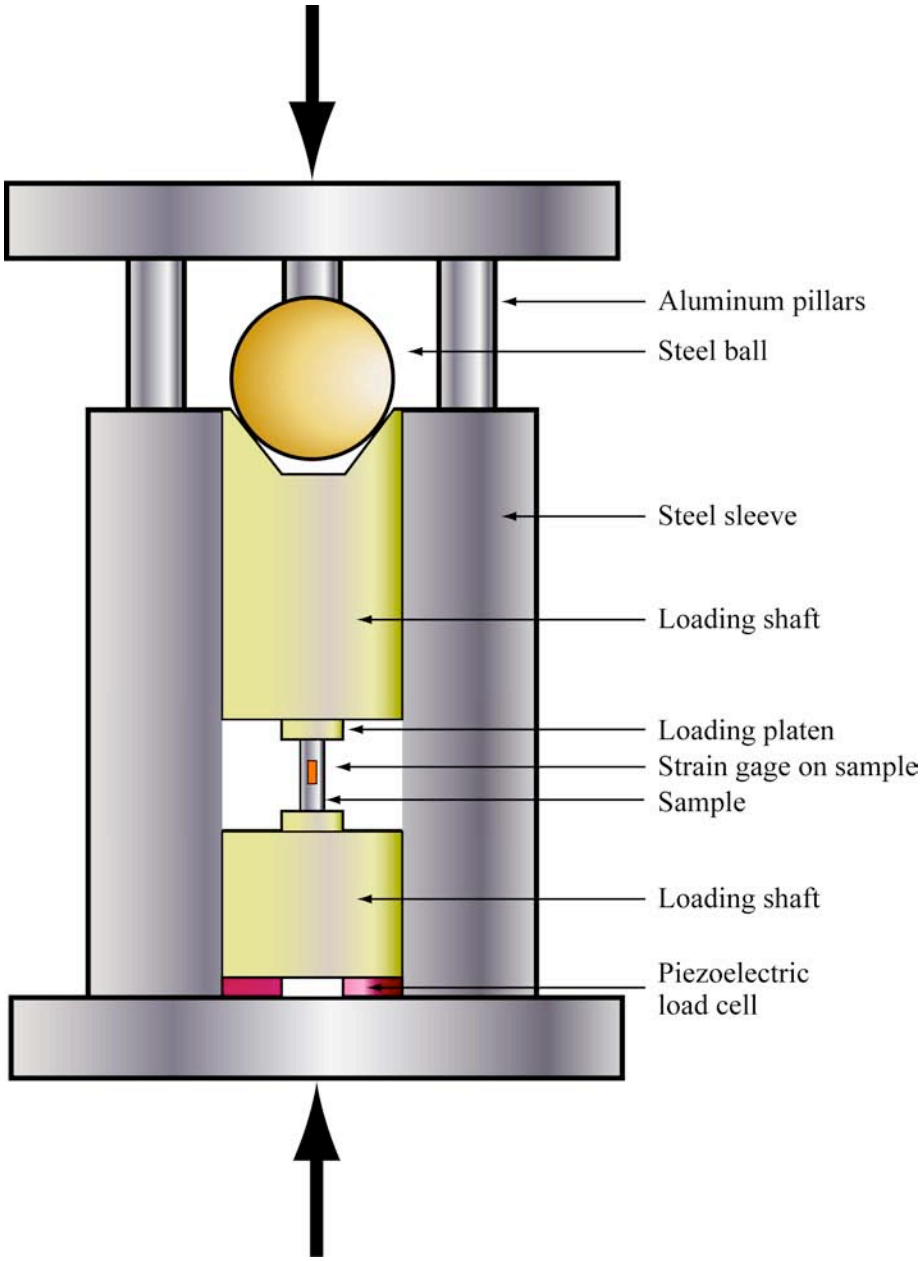

Figure 1. A schematic diagram of the load train used to compress the $Pd_{40}Ni_{40}P_{20}$ bulk metallic glass samples. The load train is shown in cross–section. Note that the drawing is not to scale.

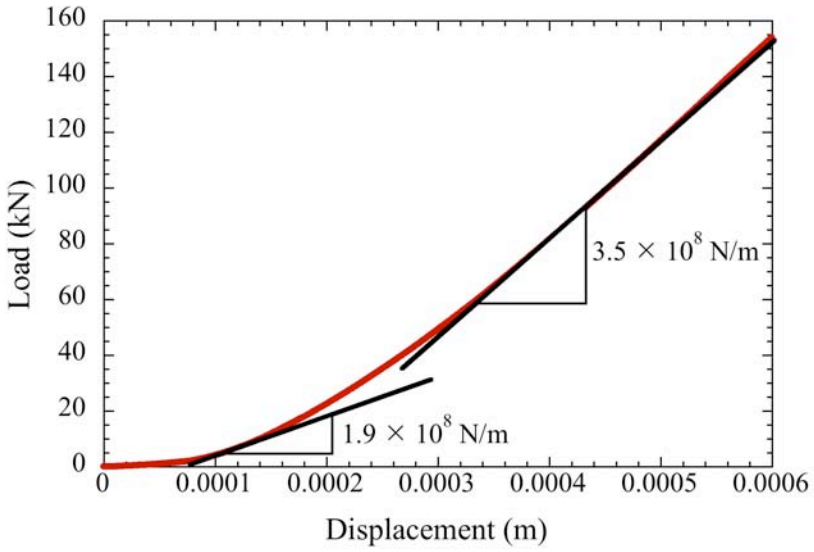

Figure 2. The load frame stiffness for the Instron 1127, demonstrating the bilinear nature of the load frame stiffness.

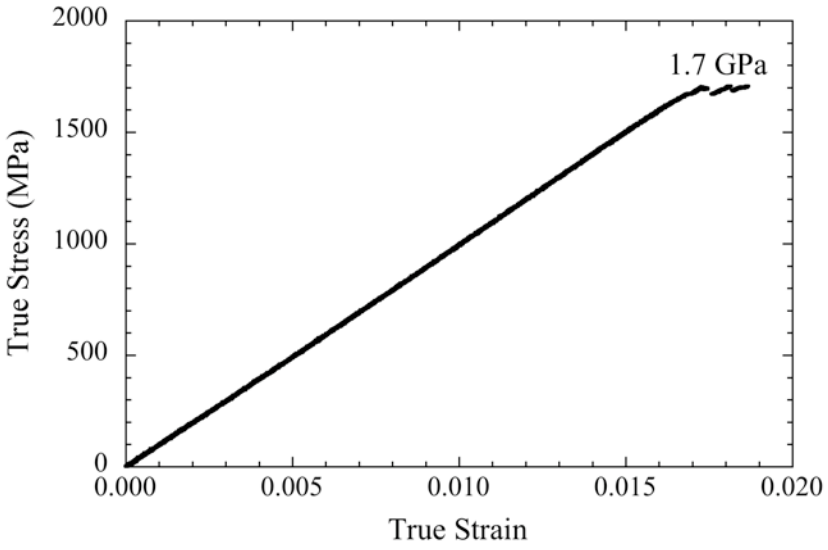

Figure 3. True stress as a function of true strain during uniaxial compression of $Pd_{40}Ni_{40}P_{20}$. The load data were acquired using the piezoelectric load cell, and the displacement data were acquired using an extensometer attached to the sample platens. The yield strength is 1.7 GPa.

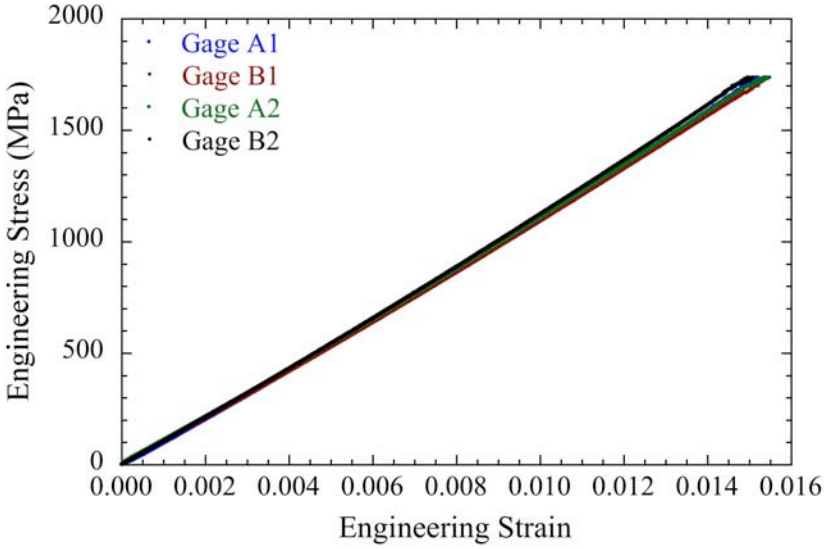

Figure 4. Engineering stress as a function of engineering strain during uniaxial compression of $Pd_{40}Ni_{40}P_{20}$ showing the data from all four strain gages. Bending of the sample was minimal as the strain recorded by the four gages differed by less than 2%.

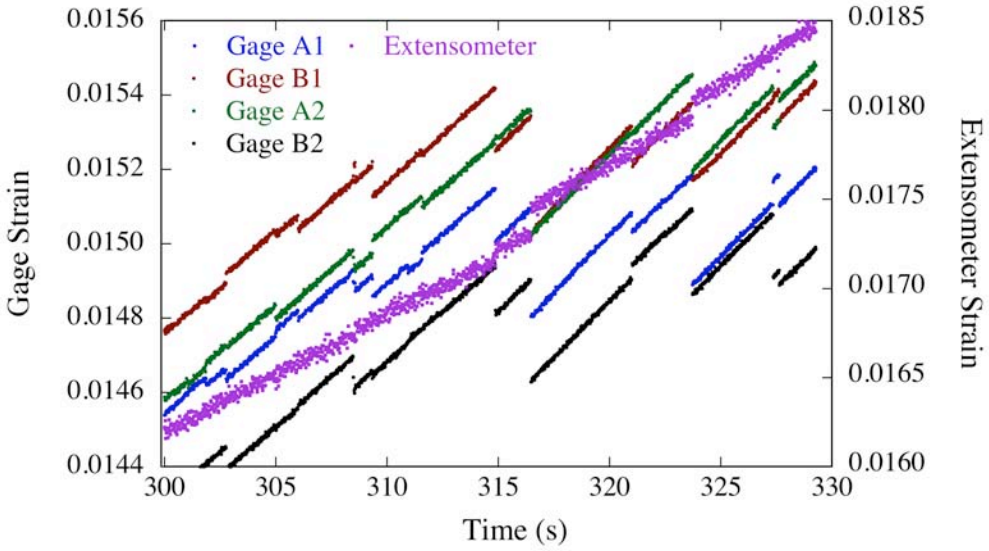

Figure 5. Engineering strain as a function of time for all four strain gages and the extensometer. Note that the extensometer strain data do not capture all of the serrations that the strain gages record.

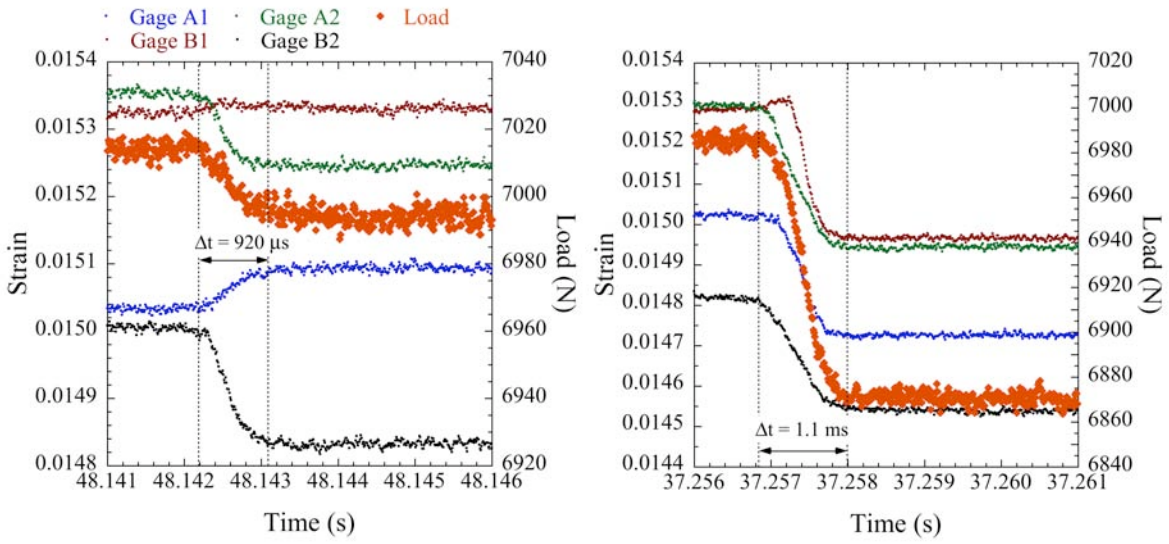

Figure 6. (a) Engineering strain as a function of time for all four strain gages and load versus time (piezoelectric load cell) for a single serration during uniaxial compression of $Pd_{40}Ni_{40}P_{20}$. The strain gages are labeled A1, B1, A2, and B2. Gages A1 and A2 were affixed to opposing sides of the sample as were Gages B1 and B2. The time is measured from the beginning of the data acquisition segment. (b) A serration in the same test.

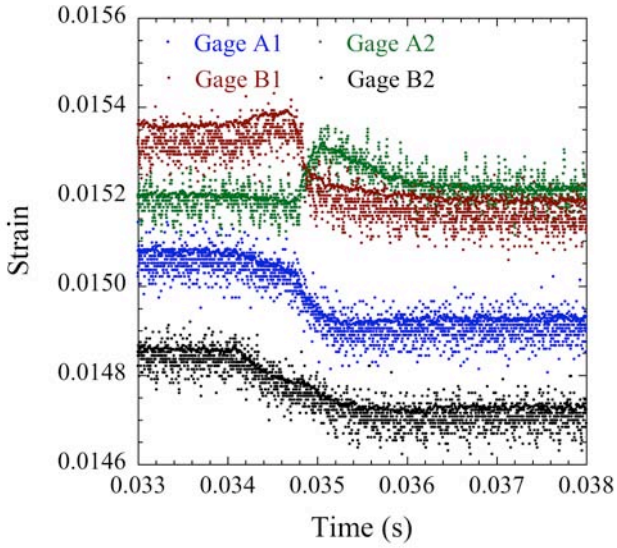

Figure 7. Engineering strain as a function of time for all four strain gages for a single serration during uniaxial compression of $Pd_{40}Ni_{40}P_{20}$. Two data sets are shown for data acquired simultaneously at rates of 100 kHz and 400 kHz. The time is measured from the beginning of the 400 kHz data acquisition segment.

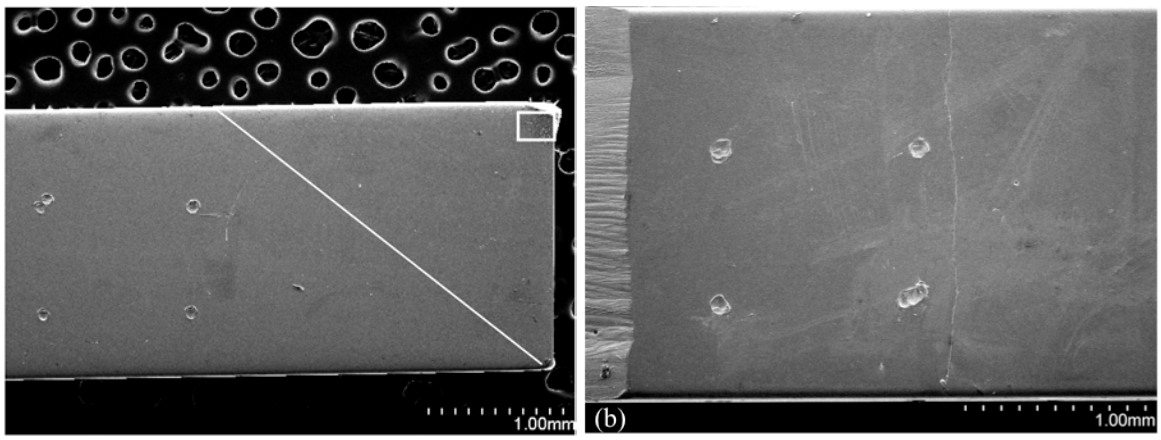

Figure 8. (a) A scanning electron micrograph of the side of the $Pd_{40}Ni_{40}P_{20}$ sample to which Gage A1 was affixed. The circular marks indicate the corners of the active grid region of the strain gage. The single intense shear band visible at this magnification does not intersect the active grid region. Note that the signal intensity of the shear band was enhanced digitally for clarity. A magnification of the region enclosed by the white rectangle is shown in Figure 9. (b) A scanning electron micrograph of the side of the $Pd_{40}Ni_{40}P_{20}$ sample to which Gage B1 was affixed. Again the circular marks indicate the corners of the active region of the strain gage, and the single intense shear band, which is the same one as seen in (a), does not intersect the active region. The fracture surface is visible on the left. The magnification of (b) is higher than the magnification of (a).

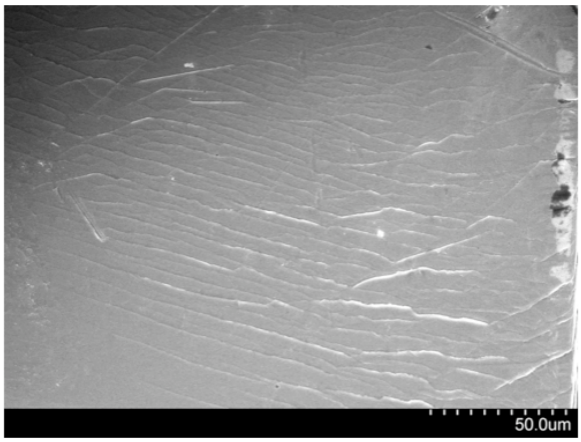

Figure 9. A magnification of the outlined region in Figure 8(a). More shear bands are observed at the sample corners than are recorded by the strain gages.

(a) (b)

Figure 10. (a) A simultaneous shear model in which the shear band operates simultaneously across the entire shear plane. For such a model, heat is generated uniformly over the shear plane as indicated by the arrows. (b) A progressive shear model for shear band propagation in which the shear band initiates at one side of the sample and then propagates progressively across it. Heat is generated in a planar process zone with width 2*a*.

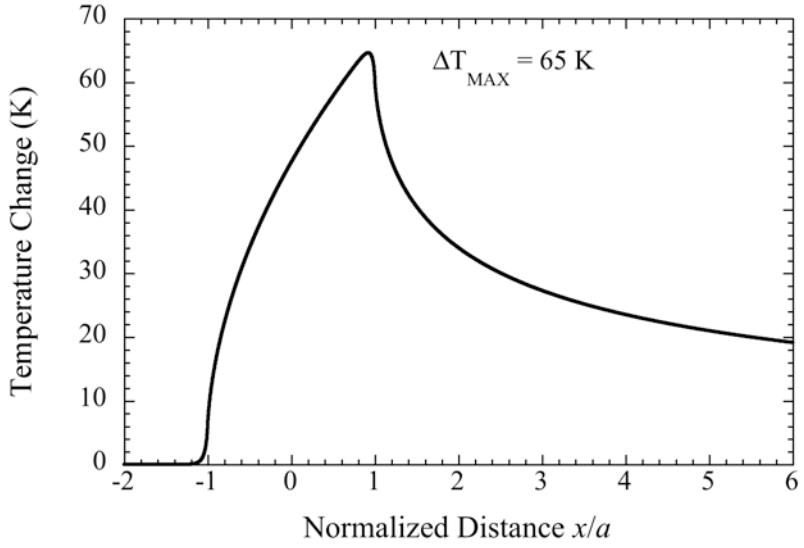

Figure 11. Temperature change in the plane of a shear band in $Pd_{40}Ni_{40}P_{20}$ as a function of distance from the heat source based on the data for a single serration in Table 1 and Equation (2). The peak temperature rise is 65 K.

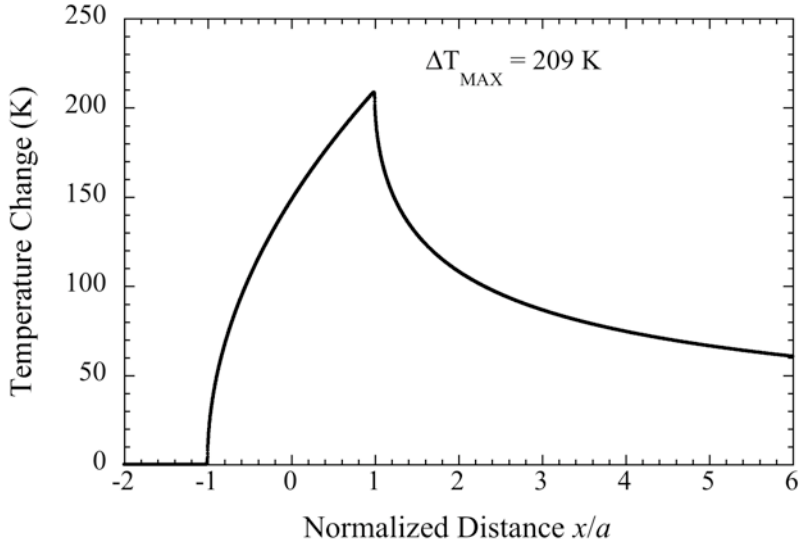

Figure 12. Temperature change in the plane of a shear band in $Pd_{40}Ni_{40}P_{20}$ as a function of distance from the heat source assuming that ten shear bands produce a single serration. The shear band propagates at a velocity ten times faster than the velocity assumed in Figure 11. The peak temperature rise is 209 K.

Table 1. A summary of the data used to produce the temperature profile in Figure 11.

Parameter	**Value**
Shear Yield Strength τ_{yield}	850 MPa
Shear Offset $u_{plastic}$	2 μm
Sample Width w	2 mm
Shear Band Orientation φ	42°
Elapsed Time Δt	1 ms
Shear Modulus μ	36.6 GPa
Thermal Conductivity K	7.03 W/(m–K) [50]
Thermal Diffusivity κ	2.16 mm^2/s [50]